Retraction Notice

The Editor-in-Chief and the publisher have retracted this article, which was submitted as part of a guest-edited special section. An investigation uncovered evidence of systematic manipulation of the publication process, including compromised peer review. The Editor and publisher no longer have confidence in the results and conclusions of the article.

RFA did not agree with the retraction.

Efficient intelligent compression and recognition system-based vision computing for computed tomography COVID images

Rabab Farhan Abbas *
University of Technology - Iraq, Department of Production and Metallurgy Engineering, Baghdad, Iraq

Abstract. Computed tomography (CT) image-based medical recognition is extensively used for COVID recognition as it improves recognition and scanning rate. A method for intelligent compression and recognition system-based vision computing for CT COVID (ICRS-VC-COVID) was developed. The proposed system first preprocesses lung CT COVID images. Segmentation is then used to split the image into two regions: nonregion of interest (NROI) with fractal lossy compression and region of interest with context tree weighting lossless. Subsequently, a fast discrete curvelet transform (FDCT) is applied. Finally, vector quantization is implemented through the encoder, channel, and decoder. Two experiments were conducted to test the proposed ICRS-VC-COVID. The first evaluated the segmentation compression, FDCT, wavelet transform, and discrete curvelet transform (DCT). The second evaluated the FDCT, wavelet transform, and DCT with segmentation. It demonstrates a significant improvement in performance parameters, such as mean square error, peak signal-to-noise ratio, and compression ratio. At similar computational complexity, the proposed ICRS-VC-COVID is superior to some existing techniques. Moreover, at the same bit rate, it significantly improves the quality of the image. Thus, the proposed method can enable lung CT COVID images to be applied for disease recognition with low computational power and space. [DOI: 10.1117/1.JEI.32.2.021404]

Keywords: region of interest; computed tomography; fast discrete curvelet transform; COVID; compression; vector quantization.

Paper 220396SS received Apr. 26, 2022; accepted for publication Jul. 6, 2022; published online Jul. 25, 2022; retracted Jun. 24, 2023.

1 Introduction

The use of computerized algorithms for image analysis in any application is referred to as image processing. The novel coronavirus (nCoV-2019), which originated in Wuhan, China, is related to the MERS and SARS virus families.[1] The computed tomography (CT) scan has been proven to be effective in detecting COVID-19. Different modalities of medical imaging are utilized to aid in the detection and analysis of disorders in the human body in the modern global environment.[2]

The number of patients treated each year is expected to increase, thereby increasing the amount of medical data collected. Furthermore, a medical image is larger than a normal image; thus, considerable data storage capabilities are necessary for medical imaging.[3] Patient medical information is sent from a multispecialty hospital to a local hospital via telemedicine infrastructure. This information is stored in a file at the hospital for future use. However, medical photographs are large or may be in the bmp format. A large number of photographs are produced for each patient in a multispecialty hospital.[4]

The hospital uses 5 to 15 gigabytes of storage space every day owing to the volume of photos it creates. Because hospitals are required to preserve each patient's medical records, managing their data storage systems is extremely difficult. Furthermore, sending photos across the network requires a large amount of bandwidth. This has the potential to increase transmission cost. Many

*Address all correspondence to Rabab Farhan Abbas, rabab.f.abbas@uotechnology.edu.iq

network challenges exist in rural areas, which may create data-transmission problems. Compression has been introduced to address these problems. The images are compressed to make them smaller.[5] Image compression can be of two types: lossy and lossless.

The lossy technique is used in applications where data loss may be tolerated, whereas the lossless technique is required when data loss cannot be tolerated, such as in the medical industry. This paper proposes a lossless compression method for medical photos and compares it to existing approaches, such as scalable RBC and integer wavelet transform (IWT). The proposed approach uses two compression techniques: fractal for image non-ROI parts and a context tree for image parts that cannot tolerate any loss.

CT is an effective noninvasive tool for the monitoring and diagnosis of COVID-19. The CT features of COVID-19 pneumonia are consolidative opacity and ground-glass opacity (GGO) affecting the bilateral and peripheral lung.[6] CT symptoms change over time as the illness progresses. Nevertheless, the patterns of post-treatment CT images following the conversion of reported nucleic acid tests are crucial not only for understanding the pathophysiology but also for creating management strategies. We analyzed chest CT scans of COVID-19 patients whose nucleic acid test results were negative after therapy to provide new data and guidelines for assessing COVID-19 remission.

Figure 1[7] shows an example of a CT images. (a) A 56-year-old woman with moderate COVID-19. Both lungs show pulmonary fibrosis (box). (b) A 37-year-old man with moderate COVID-19. The opacity of the mixed ground glass can be seen in this CT scan (box). (c) A 32-year-old woman with moderate COVID-19.

Pleural thickening and adhesion can be observed on the CT scan (arrow). (d) A 50-year-old woman suffering from severe COVID-19. GGOS were observed in both lungs (box) on CT scan. (e) A 59-year-old woman with severe COVID-19.

In the right lung, consolidation with an air bronchogram (arrow) and GGOs (box) are seen. (f) A 65-year-old man with severe COVID-19. Bronchiectasis and thickening of the bronchial wall can be seen (black arrow). There is also evidence of vascular enlargement (white arrows). Both lungs show pulmonary interstitial reticular thickening, as shown in the two boxes.

This paper is organized into four sections. The first contains an introduction, the second covers previous research, and the third provides the materials and procedures for the relevant approaches. The results and comments are presented in the fourth part. The conclusions of the proposed system are presented in the final part of the paper.

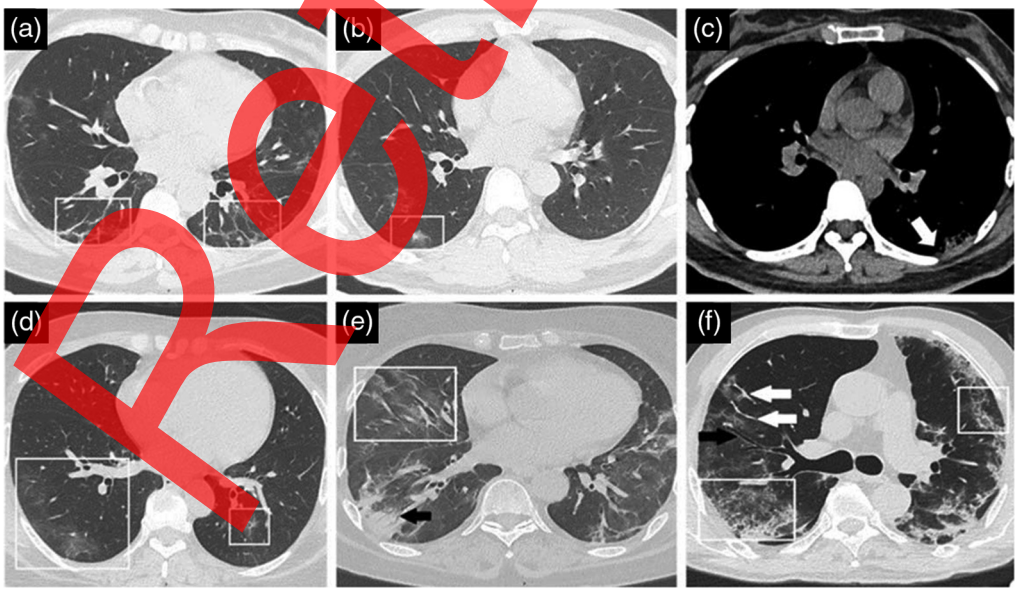

Fig. 1 Lung CT images of COVID-19 patients: (a) a 56-year-old woman, (b) a 37-year-old man, (c) a 32-year-old, (d) a 50-year-old woman, (e) a 59-year-old woman, and (f) a 65-year-old man.

2 Related Works

Suma and Sridhar[8] introduced the Huffman compression system, which conducts crossover and vertical multiplication and eliminates superfluous data without altering the image and is dependent on the Urdhava Tiryakbhyam method. By reducing the clock frequency, the power consumption for compressing color and gray medical images is increased. In addition to the transformation approaches, Huffman's method was employed in Refs. 9 to 11. Furthermore, fractal approaches and Liu et al. [12] applied the Huffman technique. The digital imaging and communications in medicine (DICOM) format is used with medical images in MRI and CT, and Yao et al.[13] developed a compression of the lossless approach on the basis of the image's differential probability.

The length of the compression code can be reduced using this differential approach, which decreases the required values of the Huffman coding number to reach optimal compression. Kaur and Wasson[14] devised a compression method that included two strategies. The region of interest (ROI) and non-ROI portions of the medical images were separated. The ROI component was compressed without loss, using a context tree. This method divides the picture into blocks set and then divides each block into four small blocks. Then, every block is compared with its parent to find the most comparable blocks to compress, and this process is repeated for the remaining block.

Liu et al.[12] suggested a fractal-technique-based MRI image compression method. The suggested approach involves converting images from a three-dimensional (3D) to two-dimensional (2D) series of images. The domain and range are classified according to the underlying spatio-temporal similarity of the 3D objects. Rahman et al.[15] proposed using the adjacent peer to the sum of absolute difference mapping to speed up the full-search fractal image (FIC) while still retaining picture quality. Shivaputra et al.[16] used an IWT to compress a DICOM file and then encrypted it with an Advanced Encryption Standard technique before sending it over a TCP/IP network.

Venugopal et al.[17] proposed a procedure that analyzes the colored medical image using low- and high-coefficient wavelets before sending each transaction to be compressed. High transactions are submitted to ripplet transformation before being compressed by Huffman, but low transactions are compressed immediately by Huffman. For medical image compression sequences, Suresh and Ukrit[18] presented a hybrid approach. To obtain a high compression ratio, the proposed method integrates the superspatial prediction technique with interframe coding and the Bose–Chaudhuri–Hocquenghem codes of the revolutionary scheme.

Sabeenian and Anandan[19] suggested a method for dividing a medical image into three stages using a rapid discrete curvelet transform (DCT) and a wrapping technique. To obtain the coefficients, the generated data were vector-quantized at each stage. Sharma et al. [20] proposed a procedure that is based on dividing the image into places of major importance (ROI) and minor importance (non-ROI) and then gathered the two transformation algorithms: for the ROI part, the set partitioning in hierarchical trees (SPIHT) algorithm, and for the non-ROI part, the Daubechies wavelet transform algorithm to produce the least amount of unnecessary data (which is deleted) to reconstruct the original image. Mofreh et al.[9] proposed a new picture compression approach that combined linear predictive coding (LPC), dual tree wavelet transform (DWT), and Huffman coding techniques.

First, the image is transformed using the LPC algorithm, wavelet transformation is applied to the LPC result, and the wavelet coefficient is coded using Huffman. The MRI compression arithmetic coding technique and the dual tree wavelet transform (DTWT) were proposed by Vaishnav et al.[21] The continuous wavelet transform is a recent improvement in DWT, with important additional properties. Abdelghany et al.[22] proposed a hybrid compression approach to compress a mammogram image that takes advantage of DCT and DWT features. The image is first compressed using three-level DWT, then modified using a one-dimensional DCT, and finally encoded using an arithmetic encoder. For medical image compression, Parikh et al.[23] proposed a high-efficiency video coding approach.

The compression method consisted of two steps: picture-format conversion and image compression. Ramya and Priya[24] proposed a DICOM compression approach that splits the picture into two sections (non-ROI and ROI) utilizing fuzzy C-means clustering. The DWT decomposes and compresses the ROI section containing the most significant data by utilizing the SPIHT

coder, keeping the image quality close to the original. The context adaptive variable length coding compression method is used to compress the N-ROI section with less significant data. For 3D medical image compression, Mishra and Himani[25] presented fast block handling using the DCT method. The DCT is used to induce image changes first and foremost. The images were divided into several sections using the DCT method. Block processing activities were conducted on 8×8 image chunks instead of processing complete images.

3 Materials and Methods

The materials and methods required by the proposed IRS-VC-COVID system are presented in this section.

3.1 *Region of Interest*

The medical images were partitioned into three sections. ROI (interest region), non-ROI, and background are the three types. Each component has its own benefits. The ROI is the most important component of the picture, covering only a small area of the images. Non-ROI is supplied so the user can quickly identify the most important region of the image. The backdrop, which is separated from the image content, is the most overlooked component of the image. These crucial areas of the image have been compressed with high quality without causing any image loss in the medical profession. For telemedicine applications, the crucial elements of the image are delivered first or at a higher priority during transmission.[26]

3.2 *Theory of Curvelet Transform*

Wavelets and ridgelets are combined to generate a curvelet transform. The wavelet transform is used to divide images into different scale sub-bands, and then a localized ridgelet transform is performed for every sub-band. Then, using a sparse coefficient set and curvelet basis, curvelets may depict a variety of scales with high-frequency contours. The curvelet transform has been shown in Fig. 2, which comprises three phases: (1) decomposition of the image, (2) smooth segmentation, and (3) ridgelet transformation:[27]

a. Image decomposition: A 2D isotropic wavelet transform is used to break down each band image into sub-bands based on resolution. Details of various frequencies are contained in each layer.
b. Smooth partitioning: The low frequency of the first layer can be described using wavelets in a smooth manner. However, it is ineffective for representing high-frequency curved features. Curvelets were used to represent the high-frequency characteristics. Each

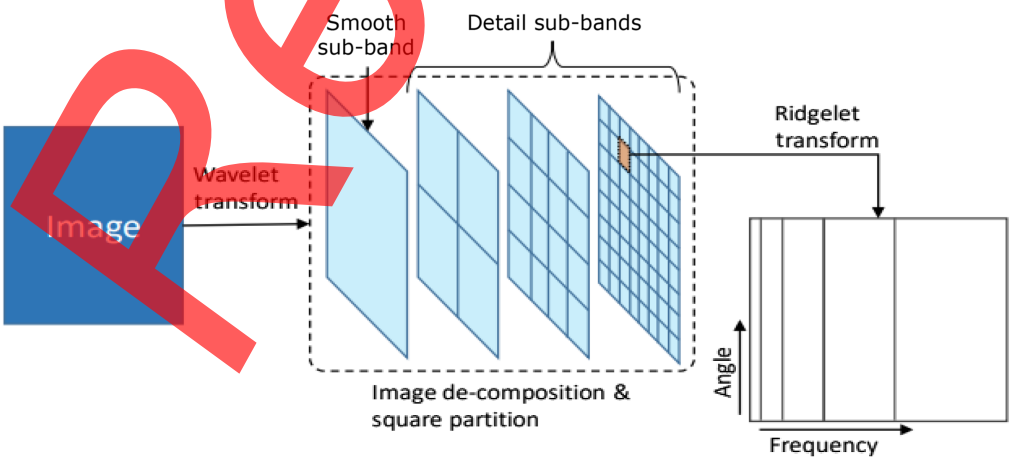

Fig. 2 Illustration of curvelet transform.

sub-band is partitioned into square partitions of an adequate scale size to efficiently express high-frequency characteristics using curvelets. Curved edges are broken down into smaller parts with smaller square partitions and are handled as straight edges on a smaller scale.

Ridgelet transform: The ridgelet transformation is applied to every square partition of every sub-band.

3.2.1 *Continuous curvelet transform*

The first wave of curvelet transforms was the continuous curvelet transform, which employed a sophisticated ridgelet transform of an image. The algorithm was modified in 2003 to improve its sluggish performance. The usage of the ridgelet transform is therefore omitted to boost the speed of the transform and decrease its redundancy. In general, all curvelet transforms can be classified into one of the three groups:[28]

a. The magnitude equals zero when the discontinuities and lengthwise supports do not intersect.
b. The magnitude is close to zero if there is an intersection between the discontinuity and lengthwise support.
c. The magnitude is greater than zero if the tangent of the discontinuity intersects the lengthwise support.

3.2.2 *Fast discrete curvelet transform*

The fast discrete curvelet transform (FDCT) is the second production transform of the curvelet (FDCT). Frequency wrapping and unequally spaced fast Fourier transform are two strategies that can be employed in FDCT implementations. Although both approaches provide the same result, the frequency wrapping method is faster to implement. The DCT method lies at the heart of the fast Fourier transform (FFT) technique, which also features multiresolution analysis. In addition, the Fourier domain is used in the convolution process of the DCT. Curvelet coefficients are created once the DCT computing procedure is completed. Both forward and inverse FFT are used to obtain the curvelet coefficients. Before using the inverse Fourier domain, a sequence of transformations is performed on the frequency tiles. Curvelet coefficients were generated using a spectral partitioning approach. It was divided into three sections: fine, detailed, and coarse. The rough, detailed, and soft levels were assigned to low, intermediate, and high frequencies, respectively.[29]

3.2.3 *Curvelet-based wrapping method*

The curvelet wrapping-based approach generally involves the following steps:[30]

a. Subjected input image to 2D FFT.
b. Divide frequency interval into digital corona tiles.
c. For each corona tile, do the following:

(i) Perform polar wedge multiplication with Fourier samples to translate the tile.
(ii) Wrap a tile-formed parallelogram around a rectangle at the origin.
(iii) Perform an inverse FFT.

Add curvelet array to the curvelet coefficients collection.

3.3 *Vector Quantization*

The encoder, channel, and decoder are the three steps of vector quantization. Figure 3 shows a schematic diagram of vector quantization. The diagram comprises three blocks, each of which works on a distinct concept. The encoder part, which comprises picture vector production,

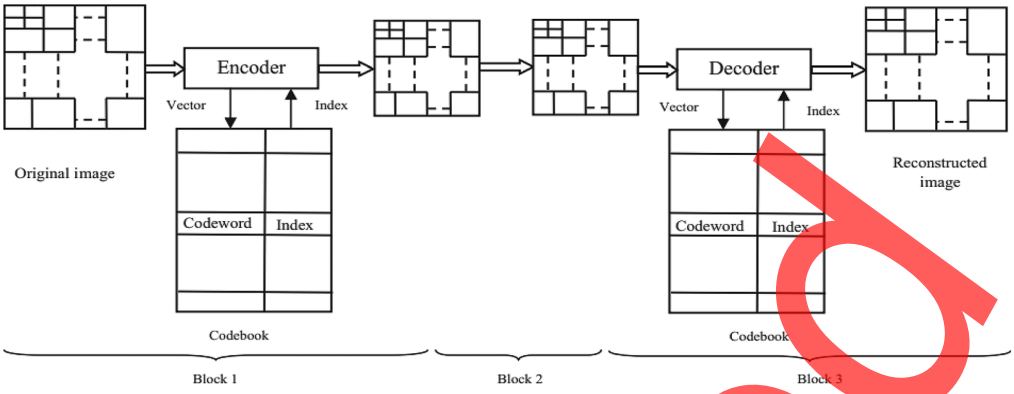

Fig. 3 Encoding and decoding processes for vector quantization.

codebook generation, and indexing, is block one. Subdividing the input image into nonoverlapping and immediate blocks yields the image vectors. The creation of an efficient codebook is the most important task.[30] A codebook is a collection of codewords of the same size as a nonoverlapping block. If the codebook created by an algorithm is efficient, it is considered superior. Every vector is labeled with an index number from the index when the codebook has been successfully generated. This information (i.e., the index number) was transmitted to the receivers. Indexed numbers are sent to the receiver through Block 2. The component of the decoder of Block3 contains an index table, codebook, and reconstructed image. The receiver index table decodes the received index numbers. The codebook of the receiver is identical to that of the transmitter. The corresponding codewords are allocated to the received index numbers, and the codewords are organized such that the reconstructed image is of the same size as the original one.[31]

3.4 *Methodology*

Preprocessing of a lung CT COVID image to eliminate noise is the first step in the current project. The images were then segmented into two uniform sections, one ROI with a context tree and the other non-ROI with fractal compression. Subsequently, FDCT compression was used to save space and bandwidth in the network. In the proposed ICRS-VC-COVID, two experiments were conducted: experiment one applied FDCT, DCT, and WT without the segmentation step; in the second experiment, these three techniques for compression were applied after the segmentation of the images. In the last step of the methodology, we applied vector quantization, as described in the previous section, with the encoding and decoding processes. Compression ratio, MSE, and PSNR were used to compare these techniques with the proposed system. The methodology of the ICRS-VC-COVID is shown in Fig. 4. Previous methods used pixel-based systems to encode images, whereas fractal compression uses image structures.

COVID-19 data must be reported. It is critical for accurately reporting case numbers and outbreaks. It is critical for identifying the most vulnerable groups of people. It is crucial for figuring out which treatments work best. It is also critical for keeping hospitals operating in the event of a pandemic.

4 Results and Discussion

MATLAB 2015a was used to create the algorithms, which were then evaluated on real-time lung CT DICOM images. A median filter was used to preprocess the data before segmentation. For all the input photos, the median filter employed a kernel size of 3×3 and a class number of 3. The input DICOM CT scans of Covid-19-affected lungs are shown in Fig. 5[32].

Due to the large scanning thickness and spacing of the CT images, the number of GGO lesions varied considerably across two adjacent image slices. Therefore, we only used the CT image slice with the greatest GGO lesion patch for each patient to reduce the impact of

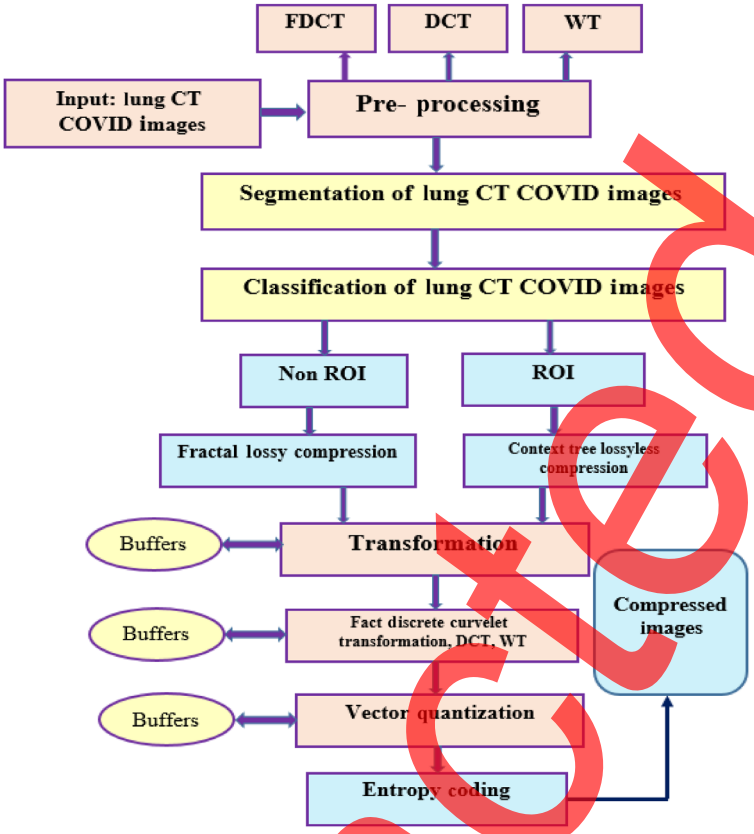

Fig. 4 Proposed ICRS-CV-COVID framework.

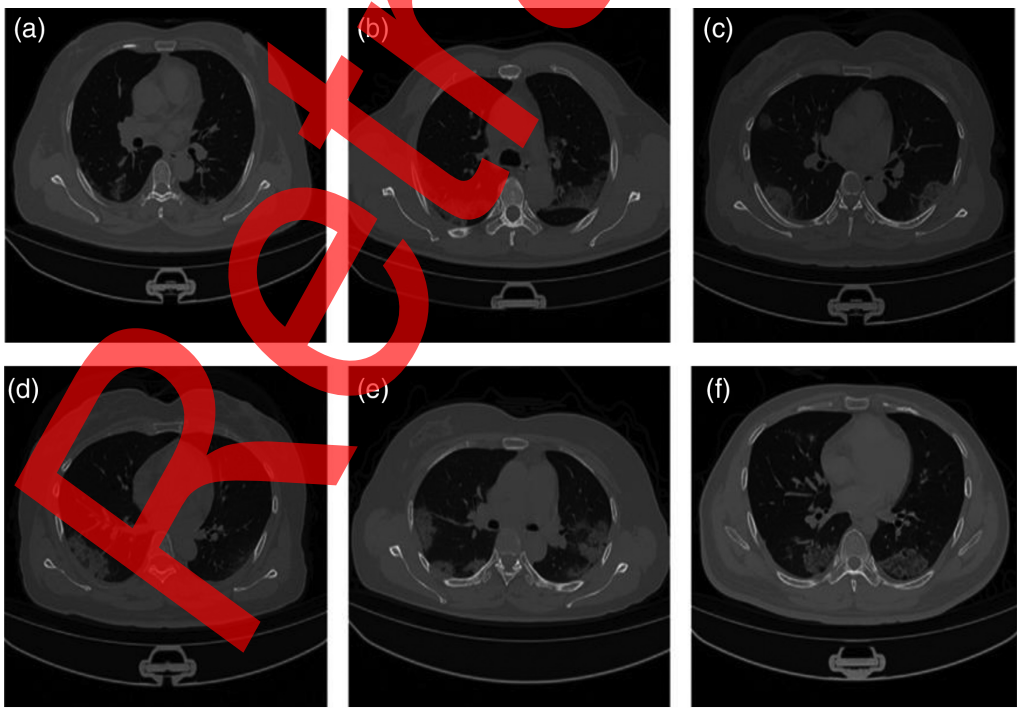

Fig. 5 Input images: (a) healthy, (b) early stage, (c) mid stage, (d) critical, (e) recovery, and (f) cured.

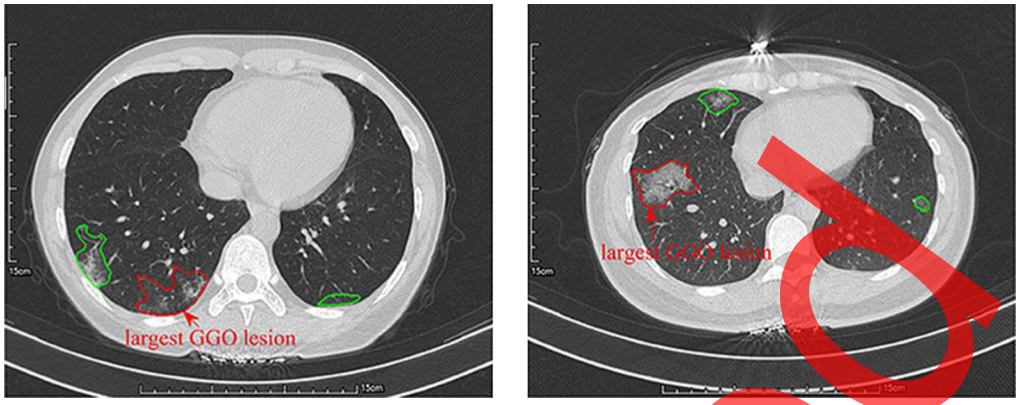

Fig. 6 Positive and negative ROI.

slice thickness and space on the study. The largest GGO lesion ROI was then identified by two radiologists in agreement with the developed custom package, both of which had more than 9 years of thoracic CT interpretation expertise, as depicted in Fig. 6.[33,34] Minor lesions are also observed in this image slice. The ROIs enclosed by the red curve are the two instances of the largest GGO lesions and were used for radiomics extracting features, whereas the areas enclosed by the green curve are other smaller lesions and were used to calculate some significant medical factors, including the position of all of the other lesions on this piece, the ratio of any of the lesion regions in the thoracic cavity on this piece, and the total number of lesions on this slice.[35,36]

The PSNR is the ratio of the maximum signal power to the undesirable noise power, the equation for it shown in Eq. (1). The signal is the true image, and the noise is the re-establishment error. A high PSNR was utilized to enhance the compression. The compression ratio is inversely proportional to the PSNR:[37]

$$\mathrm{PSNR} = 10\log_{10}\frac{R^2}{\mathrm{MSE}}. \tag{1}$$

The compression ratio and PSNR must be balanced to achieve genuine compression. The CR value is the ratio of the number of bits required to represent a genuine image to the number of bits required to represent a compressed image.

Quality is negotiated if the CR is high. Compression methods that do not lose information have a lower CR than lossy compression methods do. The MSE is the difference between the original and compressed images.

The MSE is the sum of the squares of the differences between the compressed and original images. To reduce distortion and obtain a large output value, the mean square error must be as low as possible. The essential parameters utilized for the quality of any compression technique

Table 1 Compression with wavelet transform without segmentation.

Lung CT images	PSNR (dB)	CR (%)	MSE (%)
Image 1	100.121	40.231	5.32
Image 2	100.091	40.113	5.13
Image 3	100.118	40.128	5.41
Image 4	100.677	40.901	5.59
Image 5	100.901	41.011	5.23
Image 6	101.291	42.711	5.44

Table 2 Compression with DCT without segmentation.

Lung CT images	PSNR (dB)	CR	MSE
Image 1	112.211	50.112	4.01
Image 2	112.503	50.314	4.11
Image 3	112.981	50.811	4.23
Image 4	112.571	50.324	4.71
Image 5	112.991	50.911	4.01
Image 6	112.529	50.332	4.31

Table 3 Compression with fact DWT without segmentation.

Lung CT images	PSNR (dB)	CR	MSE
Image 1	120.113	60.222	2.19
Image 2	120.281	61.091	2.33
Image 3	120.712	60.191	2.17
Image 4	121.003	60.418	2.72
Image 5	122.151	60.312	2.11
Image 6	122.441	61.712	2.51

Table 4 Compression with fractal and context tree segmentation.

Lung CT images	PSNR (dB)	CR	MSE
Image 1	130.124	70.141	1.39
Image 2	130.981	70.013	1.99
Image 3	130.112	70.112	1.42
Image 4	132.162	70.611	1.64
Image 5	131.613	70.712	1.78
Image 6	130.378	71.228	1.62

Table 5 Compression of wavelet transform with segmentation.

Lung CT images	PSNR (dB)	CR	MSE
Image 1	120.221	50.112	4.11
Image 2	120.219	49.312	4.21
Image 3	119.814	49.821	4.49
Image 4	120.118	49.113	4.22
Image 5	120.321	50.21	4.17
Image 6	118.315	50.221	4.88

Table 6 Compression of DCT with segmentation.

Lung CT images	PSNR (dB)	CR	MSE
Image 1	124.126	60.221	3.32
Image 2	123.911	60.733	3.11
Image 3	123.881	60.514	3.98
Image 4	124.542	60.291	3.21
Image 5	124.014	59.201	3.11
Image 6	122.241	60.712	3.61

Table 7 Compression with fractal, context tree, and FDCT.

Lung CT images	PSNR (dB)	CR	MSE
Image 1	240.115	80.241	0.12
Image 2	241.421	80.449	0.34
Image 3	240.011	80.114	0.91
Image 4	243.712	80.511	0.22
Image 5	242.522	81.711	0.45
Image 6	241.134	80.314	0.61

are the PSNR and CR. The PSNR and CR for six lung CT COVID images were calculated using the suggested framework (FDCT, fractal, and context tree) and compared to FDCT, WT, and DCT without segmentation. Tables 1–7 compare the performance metrics. Figures 7–13 are also included.

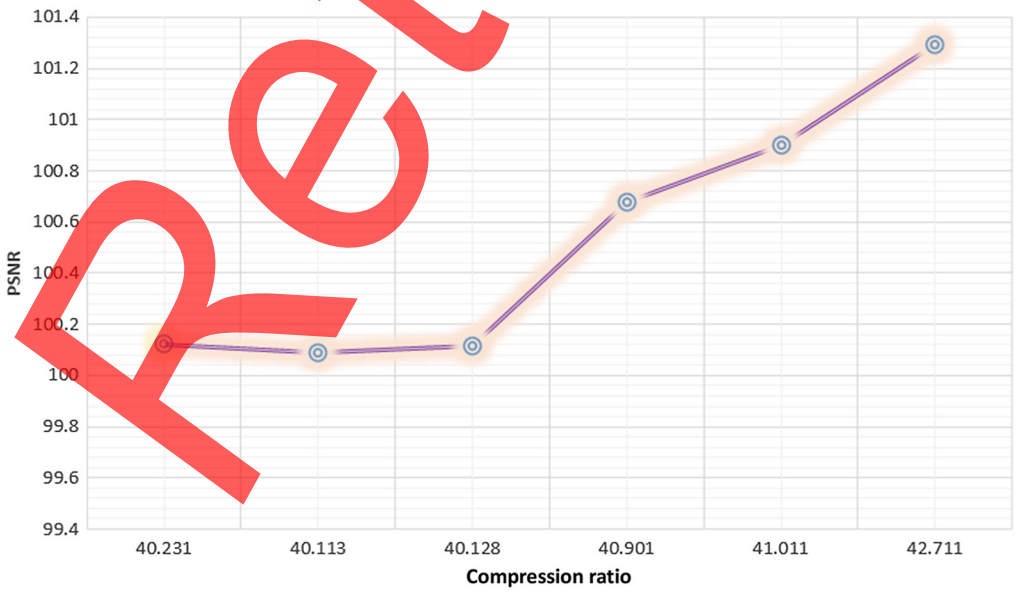

Fig. 7 Compression with wavelet transform without segmentation.

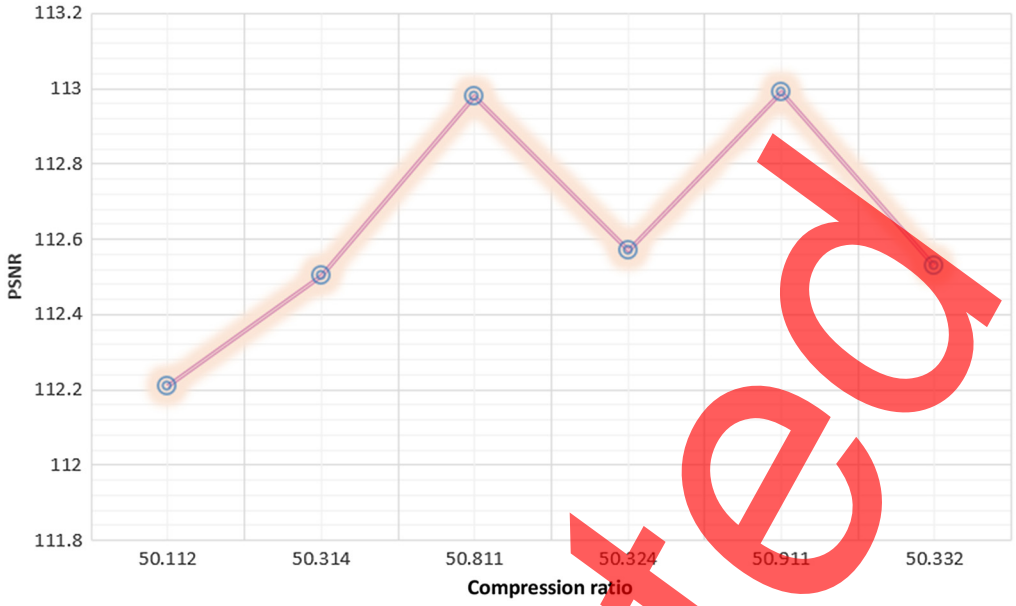

Fig. 8 Compression with DCT without segmentation.

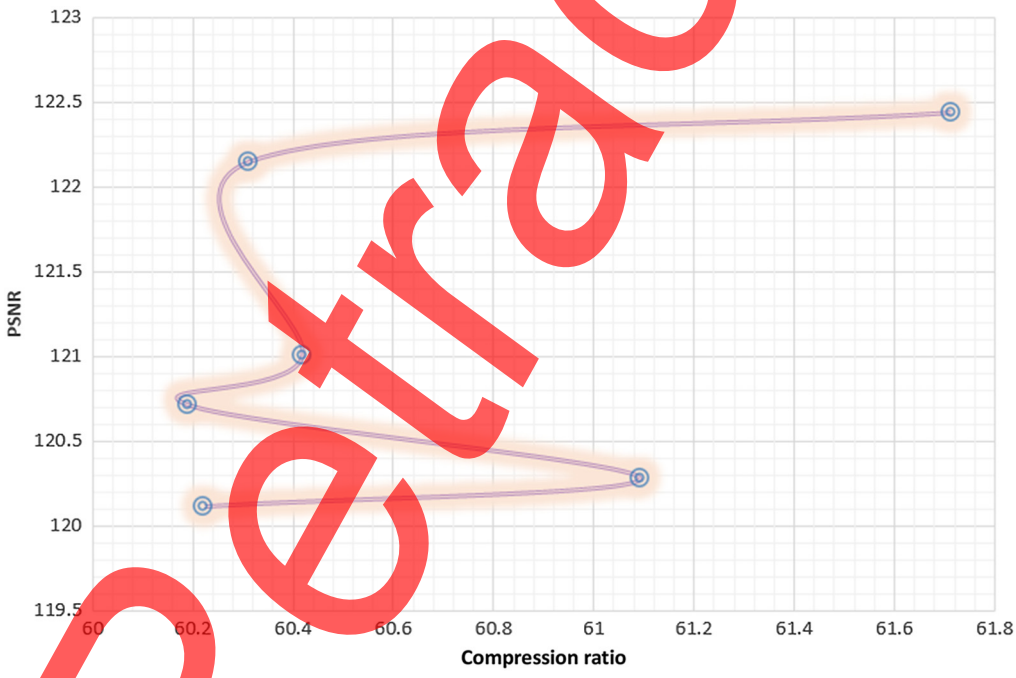

Fig. 9 Compression with fact DWT without segmentation.

5 Conclusions

In this study, an ICR-VC-COVID system was developed. Image compression is widely used in real-time applications that send data over the internet. In this study, FDCT-based "context tree" lossless ROI compression and "fractal" compression was used for non-ROI areas. When compared to previous methods, such as WT and DCT, the proposed strategies show a high compression ratio, high PSNR, and low rate of mean squared error. Experiments showed that

Fig. 10 Compression with fractal and context tree segmentation.

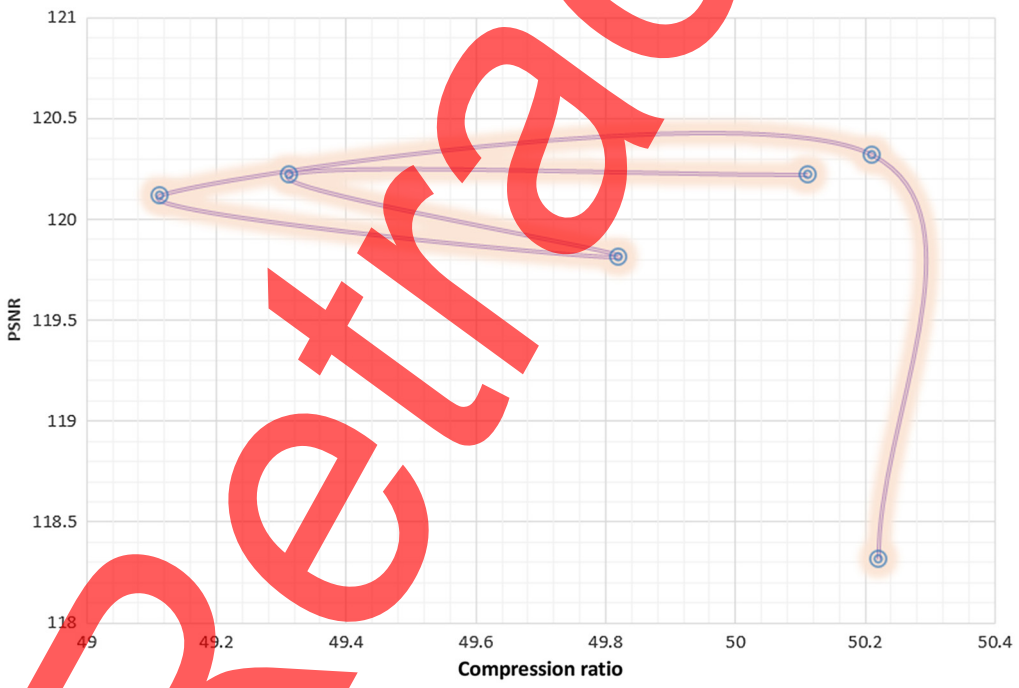

Fig. 11 Compression of wavelet transform with segmentation.

the fractal and context tree techniques are faster and more accurate than the previous ones. Although this study is a review of similar research, it provides insight into various uses. Further research will enable curvelets to be used in a variety of sectors, including medical imaging. Various COVID images of the lungs were utilized to validate the suitability of the ICR-VC-COVID system for use in medical imaging.

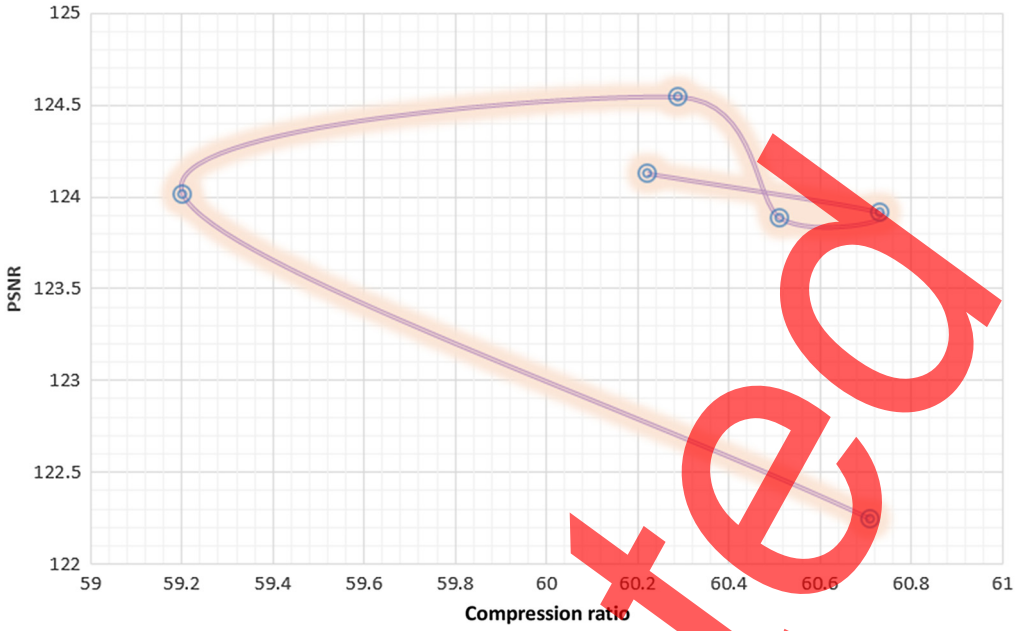

Fig. 12 Compression of DCT with segmentation.

Fig. 13 Compression with fractal, context tree, and FDCT.

References

1. V. Wiley and T. Lucas, "Computer vision and image processing: a paper review," *Int. J. Artif. Intell. Res.* **2**(1), 22–36 (2018).
2. B. N. Adday et al., "Enhanced vaccine recommender system to prevent COVID-19 based on clustering and classification," in *Int. Conf. Eng. and Emerg. Technol. (ICEET)*, IEEE (2021).
3. M. Narwaria et al., "HDR-VDP-2.2: a calibrated method for objective quality prediction of high-dynamic range and standard images," *J. Electron. Imaging* **24**(1), 010501 (2015).

4. A. R. Akkar and S. Salman, "Detection of biomedical images by using bio-inspired artificial intelligent," *Eng. Technol. J.* **38**(2), 255–264 (2020).
5. M. K. Oudah et al., "Improvement of image steganography using discrete wavelet transform," *Eng. Technol. J.* **38**(1), 83–87 (2020).
6. K. Purohit et al., "Covid-19 detection on chest x-ray and ct scan images using multi-image augmented deep learning model," in *Proc. Seventh Int. Conf. Math. and Comput.*, Singapore, Springer (2022).
7. Z. Fu et al., "CT features of COVID-19 patients with two consecutive negative RT-PCR tests after treatment," *Sci. Rep.* **10**(1), 1–6 (2020).
8. S. Suma and V. Sridhar, "Design of multiplier for medical image compression using Urdhava Tiryakbhyam Sutra," *Int. J. Electr. Comput. Eng.* **6**(3), 1140–1151 (2016).
9. A. Mofreh, T. M. Barakat, and A. M. Refaat, "A new lossless medical image compression technique using hybrid prediction model," *Signal Process. Int. J.* **11**(3), 20–30 (2016).
10. S. S. Jasim, "Medical images compression based on SPIHT and BAT inspired algorithms," *Iraqi J. Comput. Inf.* **45**(1), 1–5 (2019).
11. P. N. T. Ammah and E. Owusu, "Robust medical image compression based on wavelet transform and vector quantization," *Inf. Med. Unlocked* **15**, 100183 (2019).
12. S. Liu et al., "A fast fractal based compression for MRI images," *IEEE Access* **7**, 62412–62420 (2019).
13. C. Yao et al., "Lossless compression of medical images based on the differential probability of images," *Int. J. Comput.* **14**, 1–8 (2020).
14. M. Kaur and V. Wasson, "ROI based medical image compression for telemedicine application," *Proc. Comput. Sci.* **70**, 579–585 (2015).
15. N. A. Z. Rahman et al., "Enhancing fractal image compression speed using peer adjacent mapping with sum of absolute difference for computed radiography images," in *AIP Conference Proceedings* **2203**(1), 020011 (2020).
16. Shivaputra, H. S. Sheshadri, and V. Lokesha, "An efficient lossless medical image compression technique for telemedicine applications," *Comput. Appl. Int. J.* **2**(1), 63–69 (2015).
17. D. Venugopal et al., "Colour medical image compression using ripplet transform and Huffman coding," *Int. J. Adv. Inf. Sci. Technol.* **4**(2), 117–122 (2015).
18. M. F. Ukrit and G. R. Suresh, "Super-spatial structure prediction compression of medical image sequences," *Indones. J. Electr. Eng. Inf.* **4**(2), 126–133 (2016).
19. P. Anandan and R. S. Sabeenian, "Medical image compression using wrapping based fast discrete curvelet transform and arithmetic coding," *Circuits Syst.* **7**(8), 2059–2069 (2016).
20. R. Sharma, C. Kamargaonkar, and M. Sharma, "Hybrid medical image compression using Spiht and Db wavelet," *Int. J. Adv. Res. Electron. Commun. Eng.* **5**(5), 1571–1575 (2016).
21. M. Vaishnav, C. Kamargaonkar, and M. Sharma, "Medical image compression using dual tree complex wavelet transform and arithmetic coding technique," *Int. J. Sci. Res. Comput. Sci. Eng. Inf. Technol.* **2**(3), 172–176 (2017).
22. H. M. Abdelghany, M. Morsy, and M. Elzalbany, "Hybrid image compression using DWT, DCT and arithmetic coding," *Int. J. Res. Appl. Sci. Eng. Technol.* **5**(XI), 169–175 (2017).
23. S. S. Parikh et al., "High bit-depth medical image compression with HEVC," *IEEE J. Biomed. Health Inf.* **22**(2), 552–560 (2018).
24. C. Priya and C. Ramya, "Medical image compression based on fuzzy segmentation," *Int. J. Pure Appl. Math.* **118**(20), 603–610 (2018).
25. Himani and P. K. Mishra, "Medical image compression using block processing with DCT," *Int. J. Adv. Res. Comput. Commun. Eng.* **7**(3), 164–172 (2018).
26. M. Kaura and V. Wassona, "ROI based medical image compression for telemedicine application," *Proc. Comput. Sci.* **70**, 579–585 (2015).
27. M. Habib, M. Zabin, and J. Uddin, "An approach to wavelet based image denoising," *J. Comput. Intell. Electron. Syst.* **1**(1), 144–148 (2012).
28. R. Patil and S. Bhosale, "Medical image denoising techniques: a review," *Int. J. Eng. Sci. Technol.* **4**(1), 21–33 (2022).
29. Y. Zhang et al., "Image stripe noise removal based on compressed sensing," *Int. J. Pattern Recognit. Artif. Intell.* **36**(02), 2254004 (2022).

30. P. Anandan and R. S. Sabeenian, "Medical image compression using wrapping based fast discrete curvelet transform and arithmetic coding," *Circuits Syst.* **7**(08), 2059 (2016).
31. K. Chiranjeevi and U. R. Jena, "Image compression based on vector quantization using cuckoo search optimization technique," *Ain Shams Eng. J.* **9**(4), 1417–1431 (2018).
32. S. N. Kumar et al., "ROI extraction in CT lung images of COVID-19 using fast fuzzy C means clustering," in *Biomedical Engineering Tools for Management for Patients with COVID-19*, V. E. Balas, Ed., pp. 103–119, Academic Press (2021).
33. X. H. Wang et al., "Elaboration of a radiomics strategy for the prediction of the re-positive cases in the discharged patients with COVID-19," *Front. Med.* **8**, 730441 (2021).
34. S. Malekshah et al., "A zonal optimization solution to reliability security constraint unit commitment with wind uncertainty," *Comput. Electr. Eng.* **99**, 107750 (2022).
35. S. Malekshah et al., "Reliability-driven distribution power network dynamic reconfiguration in presence of distributed generation by the deep reinforcement learning method," *Alexandria Eng. J.* **61**(8), 6541–6556 (2022).
36. S. Malekshah and J. Ansari, "A novel decentralized method based on the system engineering concept for reliability-security constraint unit commitment in restructured power environment," *Int. J. Energy Res.* **45**(1), 703–726 (2021).
37. N. Yavarishad, "A high-bandwidth, spectrally broad photodetector based on optically-induced Seebeck effect," Doctoral Dissertation, The University of Wisconsin-Milwaukee (2021).

Rabab Farhan Abbas received her master's degree in computer science from the University of Technology, Iraq, in 2014. She received the scientific title of lecturer in 2017. Currently, she works as a lecturer in the Department of Production and Metallurgy Engineering at the University of Technology, Iraq.